INTERNATIONAL JOURNAL FOR NUMERICAL METHODS IN FLUIDS, VOL. 17, 887–904 (1993)

A MULTIGRID PROCEDURE FOR THREE-DIMENSIONAL FLOWS ON NON-ORTHOGONAL COLLOCATED GRIDS

K. M. SMITH,* W. K. COPE AND S. P. VANKA

Department of Mechanical and Industrial Engineering, University of Illinois at Urbana-Champaign, 1206 West Green, Urbana, IL 61801, U.S.A.

SUMMARY

The development of a multigrid solution algorithm for the computation of three-dimensional laminar fully-elliptic incompressible flows is presented. The procedure utilizes a non-orthogonal collocated arrangement of the primitive variables in generalized curvilinear co-ordinates. The momentum and continuity equations are solved in a decoupled manner and a pressure-correction equation is used to update the pressures such that the fluxes at the cell faces satisfy local mass continuity. The convergence of the numerical solution is accelerated by the use of a Full Approximation Storage (FAS) multigrid technique. Numerical computations of the laminar flow in a 90° strongly curved pipe are performed for several finite-volume grids and Reynolds numbers to demonstrate the efficiency of the present numerical scheme. The rates of convergence, computational times, and multigrid performance indicators are reported for each case. Despite the additional computational overhead required in the restriction and prolongation phases of the multigrid cycling, the superior convergence of the present algorithm is shown to result in significantly reduced overall CPU times.

KEY WORDS Finite-volume Non-orthogonal co-ordinates Multigrid Collocated grids

INTRODUCTION

The numerical solution of the steady incompressible flow equations on general curvilinear grids has several complexities that must be carefully addressed. The differential equations on a general curvilinear grid contain far more terms than for a rectangular grid due to the presence of co-ordinate metrics. These additional terms significantly influence the performance of any solution procedure. Also, several different formulations of the momentum equations are feasible depending on which components of the velocity vector (covariant, contravariant, Cartesian) are chosen to be the dependent variables. This choice of dependent variables directly influences the pressure–velocity coupling and, therefore, the effective rate of convergence. Since the economical solution of industrial flow problems is a primary goal of computational fluid dynamics, the overall numerical procedure should be rapidly convergent.

In developing the present numerical procedure, several staggered and non-staggered formulations of the momentum equations based on grid-oriented velocity components were considered.[1–4] Any numerical method for incompressible flow in curvilinear co-ordinates must address the issues of pressure–velocity coupling and curvature terms. Although covariant and

* Author to whom all correspondence should be addressed.

0271–2091/93/220887–18$14.00

Received 8 October 1992
Revised 3 June 1993

contravariant formulations possess strong pressure–velocity coupling, their implementation introduces curvature terms arising from the grid transformations. The presence of these terms precludes casting the equation set in conservation law form. Also, the geometric conservation law cannot be satisfied in a discrete manner when grid-oriented velocity components are used as the dependent variables.[5] Traditional staggering of the Cartesian velocity fields relative to the cell-centred pressure[6] circumvents the problems associated with grid-sensitive curvature terms; however, for grid rotations of 90°, the beneficial effect of the grid staggering may be lost under certain conditions and decoupling of the pressure–velocity fields may occur.[5] This decoupling can be overcome at the expense of storage and computational requirements by storing all three velocity components on each cell face.[7] Staggered arrangements, especially for three-dimensional applications, are tedious to incorporate into a multigrid framework due to the necessity of maintaining several individual grids throughout the restriction and prolongation phases.

The numerical formulation presented in this paper is based on a collocated arrangement of the Cartesian velocities in which the velocity components and the pressure are located at cell centres. Collocated arrangement of the primitive variables[8–10] has some obvious advantages over staggered grids, especially when non-orthogonal co-ordinates are used for the simulation of complex geometries.[11] The equation set is concise since no curvature terms are present and the scheme is completely consistent throughout arbitrary grid rotations. Since all variables are located at the cell centres, only one set of control volumes is required, thereby simplifying the development of multi-dimensional flow solvers. The convection contribution to the coefficients in the discretized equations is the same for all variables which is especially attractive when elaborate differencing schemes are employed. Additionally, boundary conditions specification is simplified since the half-grid cells encountered in staggered schemes are circumvented.

Collocated schemes offer additional advantages in a multigrid framework since only one set of control volumes requires restriction and prolongation operations. The use of the multigrid technique for accelerating the convergence of fluid flow calculations has been demonstrated by several researchers with dramatic reductions in computing times for a wide variety of numerical procedures and formulations.[12–17] However, there has been relatively little research reported for multigrid solutions of incompressible flows based on a collocated arrangement of the primitive variables.[18–20] Furthermore, these works were limited to two-dimensional rectangular domains. Recently, Demirdzic *et al.*[21] reported multigrid solutions to incompressible flows using a collocated arrangement on a generalized two-dimensional non-orthogonal grid. Since the objective of their study was to provide benchmark solutions to several challenging flows, a detailed presentation of the numerical implementation, the practices employed to make it successful, or a systematic assessment of the performance of the algorithm was not provided.

The objective of the present paper is to report the development and performance of a multigrid solution procedure for the computation of *three-dimensional* fully-elliptic incompressible flows on curvilinear collocated grids. A consistent multigrid formulation utilizing full cycling with nested iteration is presented as part of this effort. The following sections discuss the governing equations solved, detail the discretization of the governing equations, and describe the multigrid solution technique. The performance of the present algorithm for computing flows in strongly curved ducts is presented in later sections, followed by a summary of conclusions.

GOVERNING EQUATIONS

For a steady incompressible laminar flow in Cartesian co-ordinates, the conservation equations for mass and momentum may be expressed in conservative form as

$$\frac{\partial}{\partial x}(\rho u)+\frac{\partial}{\partial y}(\rho v)+\frac{\partial}{\partial z}(\rho w)=0$$

$$\frac{\partial}{\partial x}(\rho uu)+\frac{\partial}{\partial y}(\rho uv)+\frac{\partial}{\partial z}(\rho uw)=-\frac{\partial p}{\partial x}+\frac{\partial}{\partial x}(\tau_{xx})+\frac{\partial}{\partial y}(\tau_{yx})+\frac{\partial}{\partial z}(\tau_{zx})$$

$$\frac{\partial}{\partial x}(\rho vu)+\frac{\partial}{\partial y}(\rho vv)+\frac{\partial}{\partial z}(\rho vw)=-\frac{\partial p}{\partial y}+\frac{\partial}{\partial x}(\tau_{xy})+\frac{\partial}{\partial y}(\tau_{yy})+\frac{\partial}{\partial z}(\tau_{zy})$$

$$\frac{\partial}{\partial x}(\rho wu)+\frac{\partial}{\partial y}(\rho wv)+\frac{\partial}{\partial z}(\rho ww)=-\frac{\partial p}{\partial z}+\frac{\partial}{\partial x}(\tau_{xz})+\frac{\partial}{\partial y}(\tau_{yz})+\frac{\partial}{\partial z}(\tau_{zz}). \tag{1}$$

The constitutive relations governing Newtonian fluids is assumed for the viscous shear stresses. Considering a curvilinear co-ordinate system with

$$\xi=\xi(x, y, z); \quad \eta=\eta(x, y, z); \quad \zeta=\zeta(x, y, z), \tag{2}$$

the partial differential equations describing continuity and momentum can be conveniently represented in strongly conservative form as a balance of convection, diffusion, and source terms by the single equation

$$\begin{aligned}\frac{\partial}{\partial \xi}(\rho U\phi)+\frac{\partial}{\partial \eta}(\rho V\phi)+\frac{\partial}{\partial \zeta}(\rho W\phi)=&\frac{\partial}{\partial \xi}\left[\frac{\Gamma^{\phi}}{J}(q_{11}\,\phi_{\xi}+q_{12}\,\phi_{\eta}+q_{13}\,\phi_{\zeta})\right]\\&+\frac{\partial}{\partial \eta}\left[\frac{\Gamma^{\phi}}{J}(q_{21}\,\phi_{\xi}+q_{22}\,\phi_{\eta}+q_{23}\,\phi_{\zeta})\right]\\&+\frac{\partial}{\partial \zeta}\left[\frac{\Gamma^{\phi}}{J}(q_{31}\,\phi_{\xi}+q_{32}\,\phi_{\eta}+q_{33}\,\phi_{\zeta})\right]\\&+S^{\phi}(\xi, \eta, \zeta)J\end{aligned} \tag{3}$$

where Γ^{ϕ} is the diffusion coefficient and $S^{\phi}(\xi, \eta, \zeta)$ is the source term for the scalar variable ϕ. By appropriately specifying the diffusion coefficient and source term, the continuity and momentum equations can be recovered. For example, to recover the continuity equation, $S^{\phi}(\xi, \eta, \zeta)$ is set to zero since there are no mass sources and the diffusion coefficient, Γ^{ϕ}, is set to zero. Introducing these values into equation (3) yields the following expression

$$\frac{\partial}{\partial \xi}(\rho U)+\frac{\partial}{\partial \eta}(\rho V)+\frac{\partial}{\partial \zeta}(\rho W)=0 \tag{4}$$

which is the familiar strongly conservative form of the continuity equation in a curvilinear co-ordinate system. In equation (3), the Jacobian, J, and the transformation metrics, q_{ij}, are defined as

$$\begin{aligned}J&=x_{\xi}y_{\eta}z_{\zeta}+x_{\zeta}y_{\xi}z_{\eta}+x_{\eta}y_{\zeta}z_{\xi}-x_{\xi}y_{\zeta}z_{\eta}-x_{\zeta}y_{\eta}z_{\xi}-x_{\eta}y_{\xi}z_{\zeta}\\q_{11}&=(y_{\eta}z_{\zeta}-y_{\zeta}z_{\eta})^2+(x_{\zeta}z_{\eta}-x_{\eta}z_{\zeta})^2+(x_{\eta}y_{\zeta}-x_{\zeta}y_{\eta})^2\\q_{22}&=(y_{\zeta}z_{\xi}-y_{\xi}z_{\zeta})^2+(x_{\xi}z_{\zeta}-x_{\zeta}z_{\xi})^2+(x_{\zeta}y_{\xi}-x_{\xi}y_{\zeta})^2\\q_{33}&=(y_{\xi}z_{\eta}-y_{\eta}z_{\xi})^2+(x_{\eta}z_{\xi}-x_{\xi}z_{\eta})^2+(x_{\xi}y_{\eta}-x_{\eta}y_{\xi})^2\\q_{12}=q_{21}&=(y_{\zeta}z_{\xi}-y_{\xi}z_{\zeta})(y_{\eta}z_{\zeta}-y_{\zeta}z_{\eta})+(x_{\xi}z_{\zeta}-x_{\zeta}z_{\xi})(x_{\zeta}z_{\eta}-x_{\eta}z_{\zeta})+(x_{\zeta}y_{\xi}-x_{\xi}y_{\zeta})(x_{\eta}y_{\zeta}-x_{\zeta}y_{\eta})\\q_{13}=q_{31}&=(y_{\xi}z_{\eta}-y_{\eta}z_{\xi})(y_{\eta}z_{\zeta}-y_{\zeta}z_{\eta})+(x_{\zeta}z_{\eta}-x_{\eta}z_{\zeta})(x_{\eta}z_{\xi}-x_{\xi}z_{\eta})+(x_{\xi}y_{\eta}-x_{\eta}y_{\xi})(x_{\eta}y_{\zeta}-x_{\zeta}y_{\eta})\\q_{23}=q_{32}&=(y_{\xi}z_{\eta}-y_{\eta}z_{\xi})(y_{\zeta}z_{\xi}-y_{\xi}z_{\zeta})+(x_{\eta}z_{\xi}-x_{\xi}z_{\eta})(x_{\xi}z_{\zeta}-x_{\zeta}z_{\xi})+(x_{\xi}y_{\eta}-x_{\eta}y_{\xi})(x_{\zeta}y_{\xi}-x_{\xi}y_{\zeta}).\end{aligned} \tag{5}$$

The contravariant velocities, U, V and W, have the physical interpretation as volume fluxes and

are related to the Cartesian velocities by

$$\begin{bmatrix} U \\ V \\ W \end{bmatrix} = [\mathbf{A}] \begin{bmatrix} u \\ v \\ w \end{bmatrix} \tag{6}$$

where the transformation matrix, **A**, is defined as

$$\begin{bmatrix} a_{11} & a_{12} & a_{13} \\ a_{21} & a_{22} & a_{23} \\ a_{31} & a_{32} & a_{33} \end{bmatrix} = \begin{bmatrix} y_\eta z_\zeta - y_\zeta z_\eta & x_\zeta z_\eta - x_\eta z_\zeta & x_\eta y_\zeta - x_\zeta y_\eta \\ y_\zeta z_\xi - y_\xi z_\zeta & x_\xi z_\zeta - x_\zeta z_\xi & x_\zeta y_\xi - x_\xi y_\zeta \\ y_\xi z_\eta - y_\eta z_\xi & x_\eta z_\xi - x_\xi z_\eta & x_\xi y_\eta - x_\eta y_\xi \end{bmatrix}. \tag{7}$$

The solution of these equations is subject to the prescription of well-posed boundary conditions as described in later sections.

NUMERICAL PROCEDURE

The governing equations are discretized by the finite-volume method and are solved in a decoupled manner. A pressure-correction equation is used to update the cell-face fluxes such that local mass continuity is satisfied. The overall solution scheme presented in this section is similar to the popular SIMPLE algorithm[22] with minor modifications to provide for adequate pressure–velocity coupling.

Discretization

The generalized transport equation (3) for a scalar quantity ϕ can be integrated over each control volume in the computational domain (see Figure 1) for an arbitrary contravariant

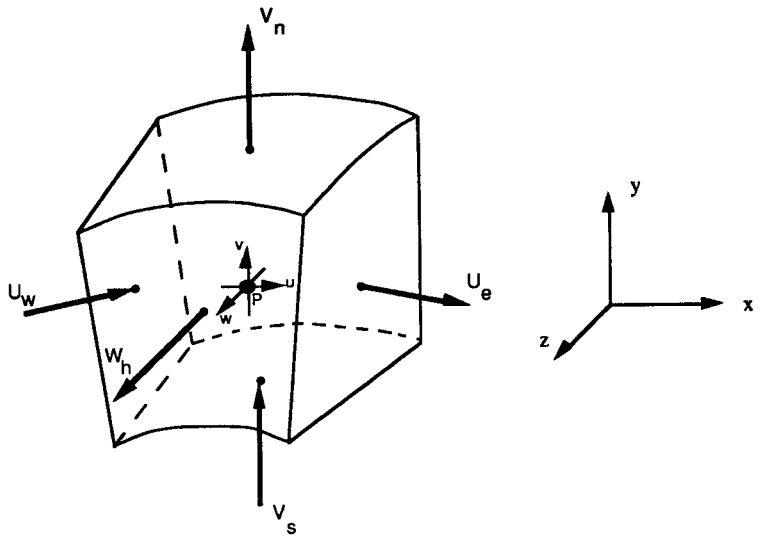

Figure 1. Typical control volume with arbitrary contravariant velocity distribution. W_t has been omitted for clarity of presentation

velocity distribution as

$$(F_e - F_w)\,d\eta\,d\zeta + (G_n - G_s)\,d\xi\,d\zeta + (H_h - H_l)\,d\xi\,d\eta = (S_1 + S_2)\,d\xi\,d\eta\,d\zeta \tag{8}$$

where

$$F = \rho U\phi - \frac{\Gamma}{J} q_{11} \frac{\partial \phi}{\partial \xi}; \qquad G = \rho V\phi - \frac{\Gamma}{J} q_{22} \frac{\partial \phi}{\partial \eta}; \qquad H = \rho W\phi - \frac{\Gamma}{J} q_{33} \frac{\partial \phi}{\partial \zeta}. \tag{9}$$

S_1 contains all cross-derivative terms and S_2 contains the integrated pressure gradient terms. The mesh increments in the computational domain are defined to be unity.

In the current version of the algorithm, the hybrid differencing[23] procedure is used for evaluating interface values of dependent variables. This discretization is known to be both stable and consistent with the governing equations.[23] Although hybrid differencing is second-order accurate when cell Reynolds numbers are less than two, its first-order accurate behavior at higher Reynolds numbers will introduce numerical diffusion. Other alternative schemes[24,25] offer formally better accuracy, however, experience has shown that they can be slow to converge and can generate over- and under-shoots in the transport variables.[26] Hybrid differencing has been used here because it offers an acceptable balance of consistency, accuracy, stability,and convergence.

After linearizing the governing equations by lagging the coefficients, the discretized transport equation can be written in the conventional algebraic form

$$A_P \phi_P = \sum_{nb} A_{nb}\,\phi_{nb} + S^{\phi} \tag{10}$$

where ϕ_{nb} are the neighbour values of ϕ_P on a seven-point stencil and S^{ϕ} is the corresponding total source term. The cross-derivative diffusion fluxes are treated explicitly by incorporating them into the source term of the discretized equation.

Pressure–velocity coupling

The key feature in collocated schemes for incompressible flows is the appropriate evaluation of cell-face velocity and pressure. In the context of a finite-volume discretization of the governing equations, values of cell-face velocity and pressure must be expressed in terms of the surrounding cell-centre quantities. When linear interpolation between cell centres is employed, the result is a discrete set of equations in which no dependence exists between adjacent cell-centre velocities and pressures. The ramification is that physically implausible velocity and pressure fields may satisfy the discrete equations.[22] The classical solution to this odd–even splitting is to use a staggered grid.[6] By staggering the control volumes, a dependence between adjacent values of velocity and pressure is obtained.

The resolution of the odd-even splitting phenomenon can be accomplished with the use of non-staggered grids. Recent solution procedures employing collocated grids incorporate grid staggering implicitly through a procedure which has been referred to as pressure weighted interpolation[27] or momentum interpolation.[28] These methods lead to well connected pressure–velocity fields in which adjacent values of velocity and pressure depend explicitly on one another.

In the present solution procedure, the method of Majumdar *et al.*[29] has been used to determine the cell-face values of the convective flux. This method was chosen in place of other collocated grid techniques because the converged solution is independent of the relaxation parameter.[28] In this formulation, values of the Cartesian velocities at the cell faces are written in terms of the

interpolated discretize equations for the adjacent cell-centre velocities. For example, if a staggered grid was being used, the east-face values u_e, v_e, and w_e would be written as

$$u_e=\left\{\frac{(\Sigma A_{nb}u_{nb})_e}{A^u_{pe}}\right\}-\left\{\frac{1}{A^u_{pe}}\right\}\left(a_{11}\frac{\partial P}{\partial \xi}+a_{21}\frac{\partial P}{\partial \eta}+a_{31}\frac{\partial P}{\partial \zeta}\right)_e+\left\{\frac{1}{A^u_{pe}}S^u(\xi,\eta,\zeta)\right\}+(1-\omega)u_e^{old}$$

$$v_e=\left\{\frac{(\Sigma A_{nb}v_{nb})_e}{A^v_{pe}}\right\}-\left\{\frac{1}{A^v_{pe}}\right\}\left(a_{12}\frac{\partial P}{\partial \xi}+a_{22}\frac{\partial P}{\partial \eta}+a_{32}\frac{\partial P}{\partial \zeta}\right)_e+\left\{\frac{1}{A^v_{pe}}S^v(\xi,\eta,\zeta)\right\}+(1-\omega)v_e^{old}$$

$$w_e=\left\{\frac{(\Sigma A_{nb}w_{nb})_e}{A^w_{pe}}\right\}-\left\{\frac{1}{A^w_{pe}}\right\}\left(a_{13}\frac{\partial P}{\partial \xi}+a_{23}\frac{\partial P}{\partial \eta}+a_{33}\frac{\partial P}{\partial \zeta}\right)_e+\left\{\frac{1}{A^w_{pe}}S^w(\xi,\eta,\zeta)\right\}+(1-\omega)w_e^{old} \quad (11)$$

where $A_p=\Sigma A_{nb}/\alpha$, and $S^u(\xi,\eta,\zeta)$, $S^v(\xi,\eta,\zeta)$, and $S^w(\xi,\eta,\zeta)$ are source terms which do not include the pressure gradients. Since a collocated grid is being considered here, quantities such as A_p and $\Sigma A_{nb}u_{nb}$ are not known at the cell faces. In the present method, a linear interpolation of the surrounding cell-centre values is employed to determine these quantities. Only those terms surrounded by braces are interpolated. It is important to note that the pressure and relaxation terms are not interpolated.

The east cell-face contravariant velocity in terms of u_e, v_e, and w_e is given by the following expression

$$U_e=a_{11}u_e+a_{12}v_e+a_{13}w_e \quad (12)$$

where a_{11}, a_{12}, and a_{13} have been calculated at the east cell-face. With the interpolation of the various terms in u_e, v_e, and w_e included, the east cell-face contravariant velocity can now be expressed in terms of cell-centre quantities as follows:

$$\begin{aligned}U_e=&a_{11}\left\{\frac{\Sigma A_{nb}u_{nb}+S^u(\xi,\eta,\zeta)}{A^u_p}\right\}-a_{11}\left\{\frac{1}{A^u_p}\right\}\left(a_{11}\frac{\partial P}{\partial \xi}+\{a_{21}\}\frac{\partial P}{\partial \eta}+\{a_{31}\}\frac{\partial P}{\partial \zeta}\right)_e\\&+a_{12}\left\{\frac{\Sigma A_{nb}v_{nb}+S^v(\xi,\eta,\zeta)}{A^v_p}\right\}-a_{12}\left\{\frac{1}{A^v_p}\right\}\left(a_{12}\frac{\partial P}{\partial \xi}+\{a_{22}\}\frac{\partial P}{\partial \eta}+\{a_{32}\}\frac{\partial P}{\partial \zeta}\right)_e\\&+a_{13}\left\{\frac{\Sigma A_{nb}w_{nb}+S^w(\xi,\eta,\zeta)}{A^w_p}\right\}-a_{13}\left\{\frac{1}{A^w_p}\right\}\left(a_{13}\frac{\partial P}{\partial \xi}+\{a_{23}\}\frac{\partial P}{\partial \eta}+\{a_{33}\}\frac{\partial P}{\partial \zeta}\right)_e\\&+a_{11}(1-\omega)u_e^{old}+a_{12}(1-\omega)v_e^{old}+a_{13}(1-\omega)w_e^{old}\end{aligned} \quad (13)$$

where the braces serve to indicate that a linear interpolation has been used to obtain that quantity. The expressions for U_w, V_n, V_s, etc. follow a similar logic.

If the terms involving u_e, v_e, and w_e in the above expression are grouped together, the resulting expression for U_e shows that it will be independent of the relaxation parameter when a converged solution is obtained. For U_e, the discretization of $\partial P/\partial \xi$ reveals the implicit grid staggering involved in the momentum interpolation procedure.[29] The expression for the cell-face mass flux, when substituted into the continuity equation to obtain a pressure-correction equation, results in dependence between adjacent values of pressure. The problem of odd–even splitting is thus avoided. Details of the implementation of this procedure for two-dimensional complex geometries can be found in Cope.[30]

Pressure-correction equation

The derivation of the pressure-correction equation follows the perturbation concept introduced by Patankar[22] in which the velocities and pressure are written as the sum of their estimated

values and a suitable correction. The pressure-correction equation takes the form

$$a_P^p p'_P = \sum_{\text{nb1}} a_{\text{nb1}}^p p'_{\text{nb1}} + \sum_{\text{nb2}} a_{\text{nb2}}^p p'_{\text{nb2}} + S^p \tag{14}$$

where the first summation includes the terms from the staggered pressure differences and the second summation includes the farther-than-neighbour values at $(i+1, j-1, k)$, $(i-1, j-1, k)$, etc. The superscript p designates the coefficients of the pressure-correction equation. Based on the recommendations of Peric,[31] the pressure gradients along the cell face resulting from the non-orthogonality of the grid lines were neglected when smoothing the pressure-correction equation since the non-orthogonality in the present study was not severe. For highly non-orthogonal meshes, the second summation in equation (14) is included and is treated explicitly during the solution of p'. The present method exhibits the best performance for geometries involving nearly orthogonal grids since the cross-derivative terms are lagged. The pressure-correction equation is swept by treating the first summation implicitly and iteratively solving the p' equation on a seven point stencil.

Integral mass flow adjustments

The convergence of the present numerical procedure can be considerably accelerated by forcing the total mass flow rate through any given cross-sectional plane to equal the known mass-flow rate. This correction is similar to the block adjustments performed in the SIMPLE technique. In the present implementation, the inflow and outflow cell-face fluxes are scaled to reflect the known mass flow rate. When the flow velocities are corrected, it is also necessary to correct the downstream pressure field to reflect the implied correction in the pressure gradient.

Smoothing operator

A vectorized alternating line Jacobi routine was employed to smooth all equation sets. In this solver, Gauss–Seidel marching was used between planes. Within a plane, direct inversion was performed in one direction with a Jacobi-like marching in the other direction. The Jacobi marching procedure eliminates interdependencies which would preclude vectorization. After one iteration of the entire flow field using inversion in the streamwise direction, inversions in the spanwise and transverse directions were performed in succession. The alternating line Jacobi solver used in the present study did not employ any explicit damping. All relaxation was performed implicitly through the discrete equations. A scalar version of a strongly implicit procedure[32] was initially used in this study, but it was not found to be computationally competitive with the alternating line Jacobi routine.

MULTIGRID PROCEDURE

Multigrid concept

Multigrid methods[33] continue to receive increased attention in the computational fluid dynamics community because of two desirable characteristics: the number of iterations is ideally independent of the number of grid cells and many problems exhibit an $O(n)$ computational effort as opposed to the $O(n^2)$ computational effort of standard single-grid iterative solvers.[20] Traditional single-grid iterative solvers are efficient in annihilating errors with wavelengths comparable to the mesh size, but their convergence for low-frequency errors is slow. Unfortunately, these low-frequency modes dominate the solution error after the first several iterations making each

successive iteration less productive.[34] In multigrid methods, a flow problem that is discretized on a given fine grid is efficiently solved by removing the persistent low-frequency errors through a series of coarse grids.

The utilization of auxiliary coarse grids serves two crucial functions in the multigrid approach. First, solutions generated on coarser grids can be extrapolated to the subsequent finer grid providing a better initial solution for the iterations on the finer grid. Second, the smooth components of the solution error, which are slow to be removed in an iterative manner, appear as high-frequency components when restricted onto a coarser grid. Several sweeps on the coarsened grid will remove the fine-grid low-frequency errors efficiently before prolongating the solution back to the finer grid. The superior convergence rate on the finest grid results in greatly reduced overall CPU times, despite the computational overhead involved in the multigrid cycling.

In the present study, the Full Approximation Storage (FAS) algorithm[33] has been combined with Full Multi-Grid (FMG) cycling to smooth the equation set. FMG–FAS cycling has been shown to provide the best convergence properties for a segregated solution of the Navier–Stokes equations,[35] especially in the presence of strongly non-linear source terms.[19] The solution procedure is initiated on the coarsest grid and subsequent initial solutions on finer grids are obtained by interpolating converged solutions of the adjacent coarser grid.

The equation set on the finest grid (k) can be written as

$$L^k w^k = F^k. \tag{15}$$

Here, L is the non-linear operator consisting of convection and diffusion terms, w is the solution vector, and F represents the source terms. In the FAS procedure, the values calculated on a coarser grid $(k-1)$ are not simple corrections to the values on grid (k), instead they are approximations on grid $(k-1)$ to the correct values on grid (k). Therefore, the equations solved on grid $(k-1)$ are

$$L^{k-1} w^{k-1} = F^{k-1} + I_k^{k-1}(F^k - L^k w^k) + (L^{k-1} I_k^{k-1} w^k - F^{k-1}) \tag{16}$$

where I_k^{k-1} is the restriction operator. Alternately, I_{k-1}^k is the prolongation operator. The correction to w^k is then calculated as

$$w^k_{\text{new}} = w^k_{\text{old}} + I^k_{k-1}(w^{k-1} - I_k^{k-1} w^k_{\text{old}}). \tag{17}$$

Note that only the change from the previous value $(w^{k-1} - I_k^{k-1} w^k_{\text{old}})$ is prolongated to grid k and not the value w^{k-1} itself. The advantage of using FAS over the Correction Scheme[33] is that the solution vector from the fine grid, and not just the residuals are transferred to the coarser grids. Additionally, if multiple iterations are performed on a coarse grid, the non-linear operator and the source terms are continuously updated.

The grid iterations can be arranged in a variety of ways which affect the overall rate of convergence. The fixed cycle is preferred here over an adaptive cycling strategy since it is not always possible to assign an optimal smoothing rate as is required in an adaptive strategy. The present study employs a fixed (ν_1, ν_2) V-cycle with ν_1 iterations during the downward leg and ν_2 iterations during the upward leg.

Treatment of coarse-grid mass fluxes

Consistent evaluation of the coarse-grid mass fluxes has been observed to be the most important issue in the present collocated multigrid procedure. If the coarse-grid cell-face fluxes are not properly updated after the momentum equations are solved, a limiting mass residual will result. Three different practices for evaluating these coarse-grid fluxes were considered in the present study.

The first method used to determine the coarse-grid mass fluxes involved the restriction of Cartesian velocities and pressure. The coarse-grid cell-face contravariant velocities were subsequently calculated from

$$\mathbf{U}^{k-1} = [\mathbf{A}]^{k-1}\,\mathbf{u}^{k-1} \tag{18}$$

where $\mathbf{U}$ is the contravariant velocity vector, $\mathbf{u}$ is the Cartesian velocity vector obtained from momentum interpolation, and $[\mathbf{A}]^{k-1}$ is the coarse-grid transformation matrix. It was observed that the first 10–15 iterations on the finest grid were consistent with a multigrid rate of convergence. The performance subsequently deteriorated to the point that no convergence was obtained below approximately 10 per cent normalized mass residual. This behaviour is attributable to a mass imbalance which exists between the coarse and fine grids when using this method.

The mass imbalance is present due to the fact that the fine-grid Cartesian velocities are not required to satisfy mass conservation.[29] Rather, it is the fine-grid cell-face fluxes based on the momentum interpolation procedure which satisfy the continuity constraint. When coarse-grid mass fluxes are calculated based on restricted Cartesian velocities from the fine grid, an inconsistency results. This inconsistency between fine and coarse-grid fluxes can be avoided by restricting the fine-grid fluxes to the coarse grid and making corrections to these restricted fine-grid fluxes at the coarse-grid level. The restricted fine-grid fluxes are only corrected on the coarse grid. The coarse-grid fluxes are never calculated based on the coarse-grid Cartesian velocities. To do so would erase the mass flux information which came down from the fine grid during restriction.

In order to resolve the observed inconsistency, a second method for calculating the coarse-grid mass fluxes was utilized. The second method involved a procedure identical to the previous method except for one important difference. The mass residual error between the fine-grid and coarse-grid fluxes was placed into the source term of the coarse-grid continuity equation. The mass residual error was calculated from

$$\dot{m}_{\text{residual}} = \Delta U_{\text{e}} - \Delta U_{\text{w}} + \Delta V_{\text{n}} - \Delta V_{\text{s}} + \Delta W_{\text{h}} - \Delta W_{l} \tag{19}$$

where

$$\Delta\mathbf{U} = I_k^{k-1}\,\mathbf{U}^k - \mathbf{U}^{k-1}. \tag{20}$$

The effect of the mass residual error was to drive the pressure corrections to remove the inter-grid mass imbalance. It was observed that a limiting mass residual of approximately 2 per cent still existed when this method was used.

In the present multigrid method, the coarse-grid mass fluxes are obtained by restricting the fine-grid fluxes to the coarse grid. The cell-face mass fluxes are calculated based on corrections to the restricted fine-grid fluxes,

$$\mathbf{U}_{\text{new}}^{k-1} = \mathbf{U}_{\text{old}}^{k-1} + [\mathbf{A}]^{k-1}\,[\mathbf{u}_{\text{new}}^{k-1} - \mathbf{u}_{\text{old}}^{k-1}]. \tag{21}$$

In this relation, the Cartesian velocity corrections are first calculated at the cell centres and then determined at the cell faces using momentum interpolation. The use of this method was observed to remove the mass inconsistency between fine and coarse grids.

Restriction/prolongation for curvilinear grids

Consistent transfer of residuals and solutions is a major aspect of any multigrid-based algorithm. For solution of the flow equations on curvilinear meshes, consistent restriction of the metrics in the governing equations is also found to be necessary. Two approaches to compute the coarse-grid transformation metrics are available: the coarse-grid metrics may be computed from the co-ordinates of the coarse-grid vertices, or the coarse-grid metrics can be a restriction of the

fine-grid metrics. The former produces metrics that do not imply the same cell-face areas and volumes as the combined values of the fine grid. In this study, improved multigrid convergence was obtained when the metrics on the coarse grids are themselves obtained by restricting the values from the adjacent finer grid.

In the present algorithm, cell-centre quantities are restricted using full weighting of neighbour values. Restriction of residuals and cell-face fluxes is performed by summation. Corrections are prolongated by trilinear interpolation.

Non-Dirichlet boundary conditions

The treatment of non-Dirichlet boundary conditions, such as symmetry planes and zero-derivative outflow planes, was performed as recommended by Vanka.[36] When a coarse grid is reached through restriction from a finer grid, it is necessary to account for the fact that the equations actually solved are different from the original flow equations because of the presence of additional restricted residuals.

TEST CALCULATIONS

General

Prior to this investigation, a detailed confirmation of the overall code, particularly the discretization consistency, was successfully performed for several model problems.[37] Because the emphasis in this study is concentrated on the implementation of a numerical procedure in a multigrid framework, comparisons of computed and experimental results are not made here. The validity of the code has been thoroughly documented elsewhere for curved duct flows in which benchmark quality experimental data are available.[37,38]

In this study, the laminar flow within a strongly curved 90° pipe bend is considered. The geometry consisted of a one diameter long approach tangent, the bend itself, and a two diameter long exit tangent. The approach tangent was included to account for any elliptic effects which might propagate upstream, while the downstream tangent was included to capture the decay of streamwise vorticity. The radius of curvature was set at 1·5 diameters. This geometry was selected because curved duct flows present several computational challenges inherent to practical engineering flows: a severe grid rotation, the possibility of localized axial recirculation, and strongly three-dimensional character. Furthermore, the present test case contains an additional challenge in that the location of the separation point is not fixed as in a sudden expansion flow.

For this configuration, three Reynolds numbers (based on the diameter and bulk velocity) of 500, 1000, and 2000 were considered. The lowest Reynolds number corresponded to a completely attached flow, while the highest Reynolds number flow was characterized by a strongly separated region in the bend. By using this range of Reynolds numbers, the performance characteristics of the algorithm could be assessed for partially-parabolic, weakly-separated, and fully-elliptic flows. For each Reynolds number, four finite-difference grids were considered to investigate the effect of grid refinement on the rate of convergence.

Because of symmetry about the central plane, only one half of the flow domain was solved. Initial velocity fields were specified as plug distributions for streamwise velocity and zero secondary circulation. The inlet boundary condition was a fully-developed Poiseuille velocity profile and an extrapolative zero-derivative outflow boundary condition was employed at the exit of the computational domain. In all cases, precautions were taken to ensure that any separated region did not extend to the outflow boundary. The streamwise and cross-sectional nodes of each

grid were distributed uniformly. A representative grid, computed using an elliptic procedure, is presented in Figure 2. The selected grid is fairly smooth, nearly orthogonal, and devoid of sudden changes in mesh size.

The convergence criterion was based on the summed average residual of the four equations defined as

$$|R| = [\sum\{(R^u)^2 + (R^v)^2 + (R^w)^2 + (R^c)^2\}/4]^{1/2} \tag{22}$$

where the summation is made over all cells. R^u, R^v, R^w, and R^c are point residuals (per unit cell volume) in the momentum and continuity equations normalized by inlet momentum and inlet mass as appropriate. A solution was considered to be adequately converged when the initial residual had been reduced by four orders of magnitude. Relaxation parameters for all grids and all Reynolds numbers were fixed at

$$\alpha_u = \alpha_v = \alpha_w = 0{\cdot}6; \qquad \alpha_p = 0{\cdot}2. \tag{23}$$

The multigrid cycling for each case contained four grid levels which were traversed using a fixed (1, 1) V-cycle with full coarsening. Each inner iteration is composed of one sweep on the momentum equations followed by five sweeps on the pressure-correction equation.

Frequent comparisons are made in this study between the relative performance of the present algorithm in single-grid and multigrid modes. In order to provide a uniform measure of computational effort, a Work Unit (WU) is defined here as one traditional single-grid iteration on the finest grid. All reported timings are actual CPU times in seconds on a CRAY-2 supercomputer.

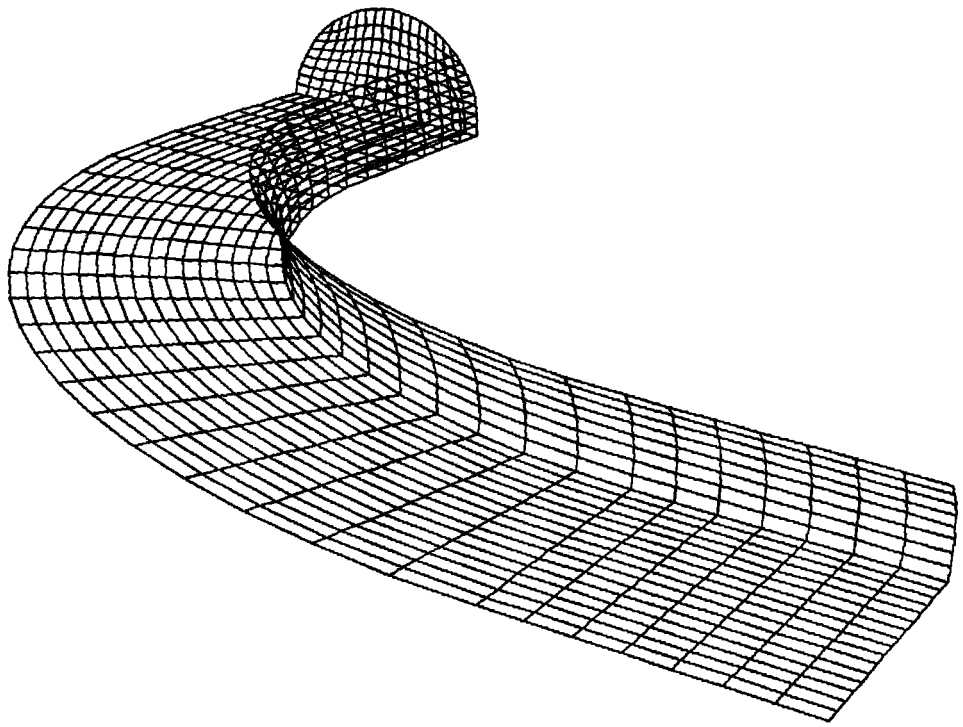

Figure 2. Representative computational grid for curved pipe simulation

Re = 500, results

As mentioned previously, no axial recirculation was observed for a Reynolds number of 500. Table I presents the results of several calculations of this flow using the same computer code in both Multi-Grid (MG) and Single-Grid (SG) modes. Clearly, the multigrid approach dramatically reduces the overall CPU times. The speedup over a traditional single-grid solver is observed to increase with grid refinement making the present multigrid procedure especially attractive for calculations involving fine grids. Although there was a small increase in the number of work units required for convergence as the grid was refined, the multigrid solution is still observed to be very economical. Single-grid calculations for the $120 \times 64 \times 40$ cell case were terminated prior to convergence since the estimated computing times would have been excessive.

Figure 3 presents the convergence histories of the various grids in the FMG cycling. Grid 1, the coarsest grid, is seen to possess the least satisfactory convergence due to the simplicity of the initial velocity field. Grid 1 converges in 53 iterations at which time the solution is prolonged to Grid 2 and the multigrid cycling begins. This convergence and prolongation pattern is repeated for Grid 3 and Grid 4. Figure 3 illustrates that the algorithm is rapidly convergent on all the grids considered.

Table I. Convergence details for curved pipe flow, $Re = 500$

Grid	MG CPU time (s)	SG CPU time (s)	CPU time speed-up	Fine grid iterations	MG work units	SG work units
$48 \times 24 \times 16$	76·1	120·8	1·59	40	59	154
$72 \times 32 \times 24$	245·7	551·6	2·25	44	64	252
$96 \times 48 \times 32$	546·9	2262·8	4·14	46	66	411
$120 \times 64 \times 40$	1232·2	6145·0*	4·99*	49	70	750*

* Estimated

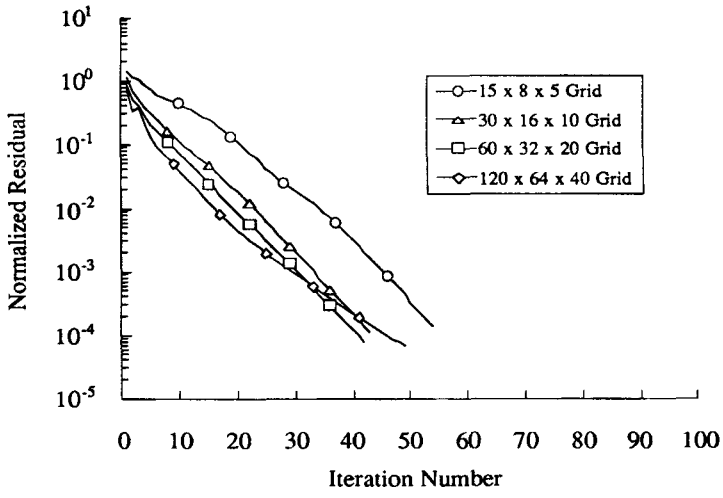

Figure 3. Convergence history for curved pipe flow, $Re = 500$

Figure 4 presents a comparison of the multigrid and single-grid convergence for the $120 \times 64 \times 40$ cell calculation. For the multigrid solution, the nested iteration phase requires approximately 8 work units. The multigrid procedure achieves final convergence in approximately 70 work units; however, over the same number of work units, the single-grid approach is seen to be very sluggish in reducing the initial residual.

$Re = 1000$, results

At a Reynolds number of 1000, the flow experiences a small separation within the first few degrees of the bend inlet. The separated region appears at the outer wall reaching a maximum backflow magnitude of 11 per cent of the bulk velocity at a bend angle of 22·5°. Table II presents performance indicators of the present algorithm for this flow. As seen in the $Re = 500$ case above, the speedup over a single-grid approach is again significant, although the speedup magnitudes are slightly less than the $Re = 500$ values for the respective grids. The increased non-linearity of this weakly separated flow is believed to be responsible for this reduced performance. The computational economy of the present multigrid method is again demonstrated by requiring only 77 work units to achieve a converged solution for the finest grid. This compares dramatically with the estimated 785 work units required by a single-grid strategy for the same flow.

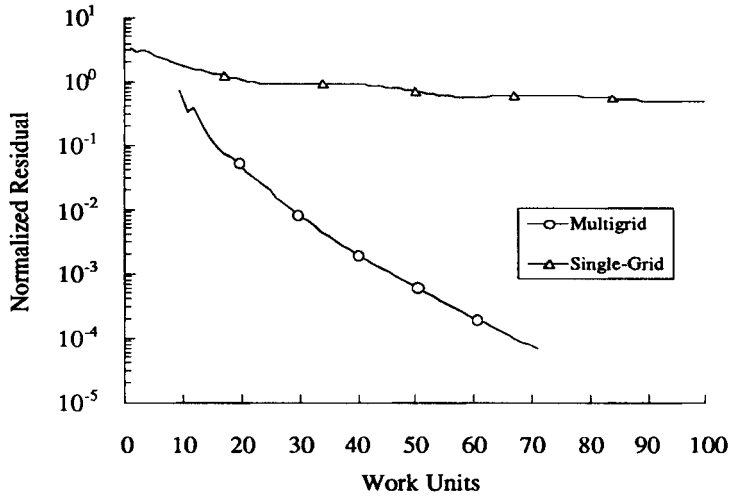

Figure 4. Multigrid and single-grid convergence history for curved pipe flow, $Re = 500$

Table II. Convergence details for curved pipe flow, $Re = 1000$

Grid	MG CPU time (s)	SG CPU time (s)	CPU time speed-up	Fine grid iterations	MG work units	SG work units
$48 \times 24 \times 16$	80·3	123·4	1·54	45	66	155
$72 \times 32 \times 24$	277·8	587·2	2·11	50	72	249
$96 \times 48 \times 32$	595·8	2211·7	3·71	52	75	408
$120 \times 64 \times 40$	1461·8	6565·0*	4·49*	54	77	785*

* Estimated

The convergence history of the FMG cycle for the $120 \times 64 \times 40$ grid calculation is presented in Figure 5. As before, the convergence on all but the initial (coarsest) grid is seen to maintain a log-linear rate. Figure 6 illustrates the convergence performance of the present algorithm in both the multigrid and single-grid modes. The multigrid method is seen to converge rapidly, while the single-grid technique appears to be converging quite slowly.

Re = 2000, results

Of the three flows considered in this study, the final flow presents the most serious challenge to the present algorithm's ability to compute practical engineering flows. At a Reynolds number of

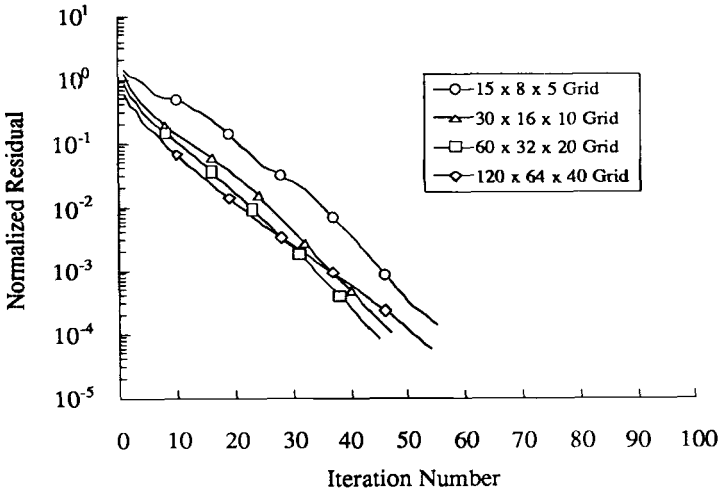

Figure 5. Convergence history for curved pipe flow, $Re = 1000$

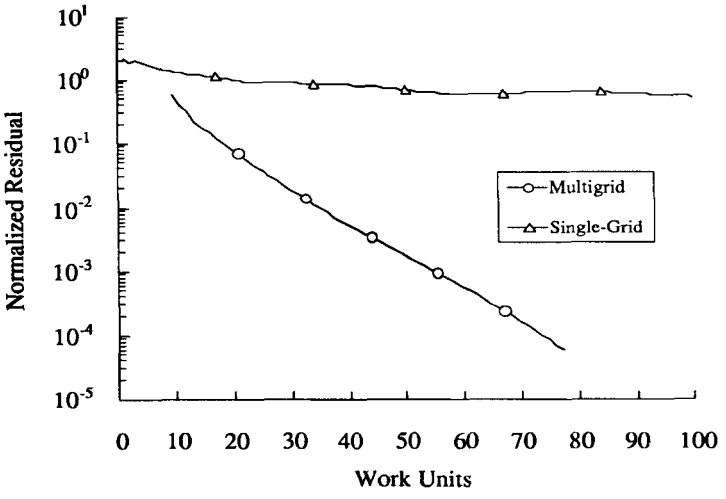

Figure 6. Multigrid and single-grid convergence history for curved pipe flow, $Re = 1000$

2000, the flow possesses a large separated region with a maximum backflow magnitude of 27·3 per cent of the bulk velocity at a bend angle of 20°. Table III presents performance indicators for this test case over a range of finite-volume grids. The speedups over a single-grid approach are still significant, but when considering the data from Tables I and II, there is a pattern of decaying speedups with increasing Reynolds number. The present multigrid method was able to achieve a fully-converged solution in less than 30 CPU min. An identical simulation using a single-grid approach was estimated to require nearly 2 CPU h. The data of Table III also indicate that the MG work units required for convergence increased appreciably as the cell density was increased. Better resolution within the separated region may be responsible for the increased MG work count as the finite-volume grids were refined.

Figure 7 presents the convergence history of the 4 level FMG cycle for the $120 \times 64 \times 40$ calculation. The four grids converge to a good accuracy essentially at the same rate. Each level in the nested iteration phase typically required only 55 iterations. The algorithm maintains strong convergence on all grids, even at this higher Reynolds number. Figure 8 illustrates the superior convergence of the multigrid cycling over an identical single-grid procedure for this Reynolds number. It is interesting to note that the 10 work units contained in the initial nested iteration accomplish approximately the same residual reduction as the 100 work units expended on a single-grid calculation.

Table III. Convergence details for curved pipe flow, $Re = 2000$

Grid	MG CPU time (s)	SG CPU time (s)	CPU time speed-up	Fine grid iterations	MG work units	SG work units
$48 \times 24 \times 16$	94·5	126·4	1·34	52	75	157
$72 \times 32 \times 24$	304·5	600·2	1·97	58	83	255
$96 \times 48 \times 32$	704·8	2461·2	3·49	60	86	429
$120 \times 64 \times 40$	1687·1	6850·0*	4·06*	66	95	810*

* Estimated

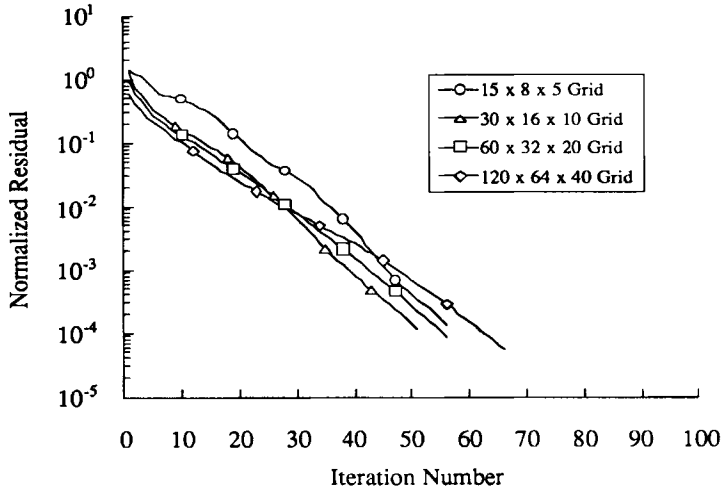

Figure 7. Convergence history for curved pipe flow, $Re = 2000$

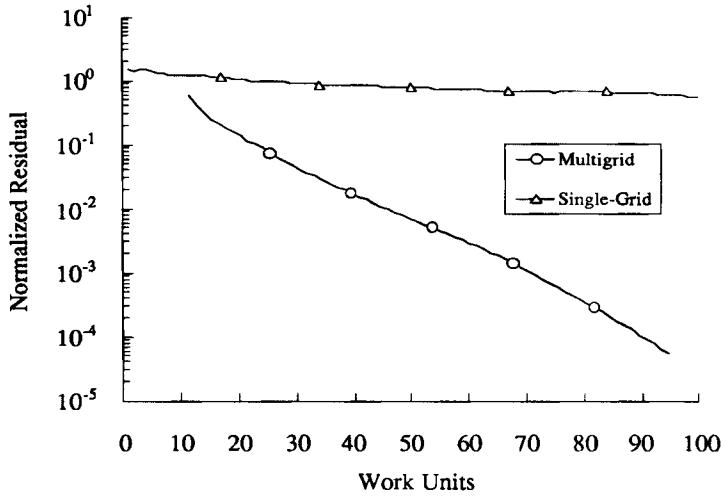

Figure 8. Multigrid and single-grid convergence history for curved pipe flow, $Re = 2000$

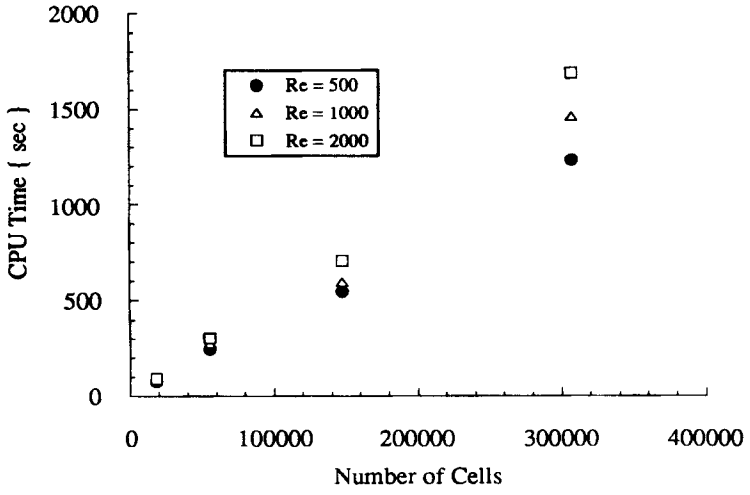

Figure 9. Effect of grid refinement on multigrid solution time

Figure 9 presents the effect of grid refinement on CPU times for all three of the Reynolds numbers considered in the present study. From Figure 9, it can be seen that the CPU time increases almost linearly with the number of grid nodes. This confirms the attractive feature of the multigrid technique. The absolute CPU time, however, increases with Reynolds number, as a result of the increased non-linearity. The present multigrid formulation approaches on $O(n)$ work count; however, the problem complexity may be responsible for not achieving this ideal multigrid efficiency. It may be possible to attain an $O(n)$ work count by tailoring the relaxation and grid cycling parameters on a case by case basis.

CONCLUSIONS

In this study, we have presented the development and performance of a multigrid-based algorithm for the solution of the steady incompressible Navier–Stokes equations. The algorithm solves the momentum equations for the Cartesian velocities as the dependent variables and stores all variables at the cell centres. In all cases, rapid convergence from initially guessed simplistic distributions has been obtained. This study demonstrates that multigrid techniques for a collocated arrangement of the primitive variables show promise for efficiently solving multi-dimensional fluid flows of practical relevance. Future research efforts are concentrated on the incorporation of turbulence modeling and higher-order discretizations for the governing equations.

ACKNOWLEDGEMENTS

The work reported here was supported by the Internal Fluid Mechanics Division at NASA Lewis Research Center under a grant to the University of Illinois. The computations were performed at the NAS facility at NASA Ames Research Center and at the National Center for Supercomputing Applications. The support of these organizations and of the NASA technical monitor, Dr. J. D. Holdeman, are gratefully appreciated. Wm. K. Cope is thankful for the support of the AFOSR through a graduate student fellowship. K. M. Smith wishes to thank Professor J. C. Dutton for his continued guidance and encouragement.

REFERENCES

1. K. C. Karki and S. V. Patankar, 'Calculation procedure for viscous incompressible flows in complex geometries', *Numer. Heat Transfer*, **14**, 295–307 (1988).
2. P. Tamamidis and D. Assanis, 'Prediction of 3-dimensional viscous flows using body-fitted coordinates', Presented at A.S.M.E. Winter Annual Meeting, December 1–6, 1991.
3. I. Demirdzic, R. I. Issa and Z. Lilek, 'Solution method for viscous flows at all speeds in complex domains', *Proc. 8th GAMM Conf. Numer. Methods Fluid Mech.*, 1990, pp. 89–98.
4. D. S. Joshi and S. P. Vanka, 'A multigrid calculation procedure for fluid flows in complex geometries', *Numer. Heat Transfer*, Part B, **20**(1), 61–80 (1991).
5. Wei Shyy and C. Vu, Thi, 'On the adoption of velocity variable and grid system for fluid flow computation in curvilinear coordinates', *J. Comput. Phys.*, **92**, 82–105 (1991).
6. Francis H. Harlow and J. Eddie Welch, 'Numerical calculation of time dependent viscous incompressible flow of fluid with free surface', *Phys. Fluids*, **8**, 2182–2189 (1965).
7. C. R. Maliska and G. D. Raithby, 'A method for computing three-dimensional flows using non-orthogonal boundary-fitted coordinates', *Int. j. numer. methods fluids*, **4**, 518–537 (1984).
8. C. M. Rhie and W. L. Chow, 'Numerical study of the turbulent flow past an airfoil with trailing edge separation', *AIAA J.*, **21**, 1525–1532 (1983).
9. M. Peric, 'A finite volume method for the prediction of three-dimensional fluid flow in complex ducts', *Ph.D. Thesis*, University of London, 1985.
10. C. F. Hsu, 'A curvilinear-coordinate method for momentum, heat and mass transfer in domains of irregular geometry', *Ph.D. Thesis*, University of Minnesota, 1981.
11. M. Peric, R. Kessler and G. Scheuerer, 'Comparison of finite-volume numerical methods with staggered and collocated grids', *Comput. Fluids*, **16**, 389–403 (1988).
12. Z. Zhu and C. A. J. Fletcher, 'Study of sequential solution for the reduced/complete Navier–Stokes equations with multigrid acceleration', *Comput. Fluids*, **19**(1), 43–60 (1991).
13. G. Juncu and R. Mihail, 'Numerical solution of the steady incompressible Navier–Stokes equations for the flow past a sphere by a multigrid defect correction technique', *Int. j. numer. methods fluids*, **11**, 379–395 (1990).
14. E. Dick, 'Multigrid method for steady incompressible Navier–Stokes equations based on partial flux splitting', *Int. j. numer. methods fluids*, **9**, 113–120 (1989).
15. S. Sivaloganathen and G. J. Shaw, 'A Multigrid method for recirculating flows', *Int. j. numer. methods fluids*, **8**, 417–440 (1988).
16. L. Fuchs and H. S. Zhao, 'Solution of three-dimensional viscous incompressible flows by a multigrid method', *Int. j. numer. methods fluids*, **4**, 539–555 (1984).
17. U. Ghia, K. N. Ghia and C. T. Shin, 'High-Re solutions for incompressible flow using the Navier–Stokes equations and a multigrid method', *J. Comput. Phys.*, **48**, 387–411 (1982).

18. M. Barcus, M. Peric and G. Scheuerer, 'A control volume based full multigrid procedure for the prediction of two-dimensional, laminar incompressible flows', in M. Deville (ed.), *Notes on Numerical Fluid Mechanics*, vol. 20, Friedr. Vieweg & Sohn Verlagsgesellschaft mbH, Braunschweig, Germany, 1988, pp. 9–16.
19. C. Becker, J. H. Ferziger, M. Peric and G. Scheuerer, 'Finite volume multigrid solution of the two-dimensional incompressible Navier–Stokes equations', in W. Hackbush (ed.), *Notes on Numerical Fluid Mechanics*, vol. 23, Friedr. Vieweg & Sohn Verlagsgesellschaft mbH, Braunschweig, Germany, 1988, pp. 37–47.
20. M. Hortmann, M. Peric and G. Scheuerer, 'Finite volume multigrid prediction of laminar natural convection: Benchmark solutions', *Int. j. numer. methods fluids*, **11**, 189–207 (1990).
21. I. Demirdzic, Z. Lilek and M. Peric, 'Fluid flow and heat transfer test problems for non-orthogonal grids: Bench-Mark solutions', *Int. j. numer. methods fluids*, **15**, 329–354 (1992).
22. S. V. Patankar, *Numerical Heat Transfer and Fluid Flow*, Hemisphere, Washington DC, 1980.
23. D. B. Spalding, 'A novel finite difference formulation for differential expressions involving both first and second derivatives', *Int. j. numer. methods eng.*, **4**, 551–559 (1972).
24. B. P. Leonard, 'A stable and accurate convection modelling procedure based on quadratic upstream interpolation', *Comput. methods appl. mech. eng.*, **12**, 59–98 (1979).
25. G. D. Raithby, 'Skew upstream differencing for problems involving fluid flow', *Comput. methods appl. mech. eng.*, **9**, 153–164 (1976).
26. M. C. Melaaen, 'Calculation of fluid flows with staggered and non-staggered curvilinear non-orthogonal grids—the theory', *Numer. Heat Transfer, Part B*, **21**, 1–19 (1992).
27. T. F. Miller and R. W. Schmidt, 'Use of a pressure-weighted interpolation method for the solution of the incompressible Navier–Stokes equations on a non-staggered grid system', *Numer. Heat Transfer*, **14**, 213–233 (1988).
28. M. Majumdar, 'Role of underrelaxation in momentum interpolation for calculation of flow with non-staggered grids', *Numer. Heat Transfer*, **13**, 125–132 (1988).
29. S. Majumdar, W. Rodi and S. P. Vanka, 'On the use of non-staggered pressure–velocity arrangement for numerical solution of incompressible flows', *SFB 210/T/35*, University of Karlsruhe, 1987.
30. Wm. K. Cope, 'On the numerical simulation of turbulent flows in complex geometries', *Master Thesis*, University of Illinois at Urbana–Champaign, 1991.
31. M. Peric, 'Analysis of pressure–velocity coupling on nonorthogonal grids', *Numer. Heat Transfer, Part B*, **17**, 63–82 (1990).
32. H. L. Stone, 'Iterative solution of implicit approximations of multi-dimensional partial differential equations', *SIAM J. Numer. Anal.*, **5**, 530–558 (1968).
33. A. Brandt, 'Multigrid techniques: 1984 guide with applications to fluid dynamics', *Monograph*, GMD-Studien, **85**, 1984.
34. S. P. Vanka, 'Block-implicit multigrid solution of Navier–Stokes equations in primitive variables', *J. Comput. Phys.*, **65**, 138–158 (1986).
35. S. P. Vanka, 'A fast numerical computation of viscous flow in a cube', *Numer. Heat Transfer, Part B*, **20**, 255–261 (1991).
36. S. P. Vanka, 'Performance of a multigrid calculation procedure in three-dimensional sudden expansion flows', *Int. j. numer. methods fluids*, **6**, 459–477 (1986).
37. K. M. Smith, 'Multigrid calculation of internal flows in complex geometries', *Master Thesis*, University of Illinois at Urbana–Champaign, 1992.
38. K. M. Smith and S. P. Vanka, 'Multigrid calculation of internal flows in complex geometries', *AIAA Paper 92-0096*, Reno, NV, 6–9 January 1992.